



Analysis of recovery efficiency in high-temperature aquifer thermal energy storage: a Rayleigh-based method

Gilian Schout · Benno Drijver ·
Mariene Gutierrez-Neri · Ruud Schotting

Abstract High-temperature aquifer thermal energy storage (HT-ATES) is an important technique for energy conservation. A controlling factor for the economic feasibility of HT-ATES is the recovery efficiency. Due to the effects of density-driven flow (free convection), HT-ATES systems applied in permeable aquifers typically have lower recovery efficiencies than conventional (low-temperature) ATES systems. For a reliable estimation of the recovery efficiency it is, therefore, important to take the effect of density-driven flow into account. A numerical evaluation of the prime factors influencing the recovery efficiency of HT-ATES systems is presented. Sensitivity runs evaluating the effects of aquifer properties, as well as operational variables, were performed to deduce the most important factors that control the recovery efficiency. A correlation was found between the dimensionless Rayleigh number (a measure of the relative strength of free convection) and the calculated recovery efficiencies. Based on a modified Rayleigh number, two simple analytical solutions are proposed to calculate the recovery efficiency, each one covering a different range of aquifer thicknesses. The analytical solutions accurately reproduce all numerically modeled scenarios with an average error of

less than 3%. The proposed method can be of practical use when considering or designing an HT-ATES system.

Keywords Aquifer thermal energy storage · Density-driven flow · Numerical modeling · The Netherlands · Thermal systems

Introduction

Thermal energy storage (TES) is considered an important energy conservation technology. It can be used when there is a mismatch between supply and demand of thermal energy. Due to the low thermal conductivity, the subsurface is very suitable for TES. Underground thermal energy storage (UTES) is mainly used for seasonal energy storage and to a lesser extent for day–night storage. The main advantage of UTES is the reduction of energy use: energy savings up to 80 % for cooling buildings and up to 30 % for heating buildings can be achieved. Important advantages that are directly related to the energy savings are the reduction of greenhouse gas emissions and cost reduction for heating and cooling. Additionally, the dependency on fossil fuels is diminished.

The two most common types of UTES are borehole thermal energy storage (BTES, also known as closed loop systems) and aquifer thermal energy storage (ATES, also known as open loop systems). ATES systems use wells that pump and inject groundwater from an aquifer. In the summer period, cold groundwater is pumped from the cold well(s). This water is used for cooling purposes and the heat released during cooling is stored in the aquifer through the warm well(s). In winter, the process is reversed in that water is pumped from the warm well(s) and applied as a heat source, e.g. as a low temperature heat source for a heat pump. After the exchange of heat, the chilled groundwater is injected into the cold well(s) again. In the Netherlands, the hydrogeological conditions for ATES are favorable and ATES is the most common type of UTES for large-scale projects (cooling/heating demand >100 kW). For such projects, ATES is favorable owing to its ability to pump large amounts of water and consequently store large quantities of thermal energy. With 1,500 registered ATES systems at the end of 2011, the Netherlands has a leading position in the world.

Received: 14 December 2012 / Accepted: 29 August 2013
Published online: 3 October 2013

© Springer-Verlag Berlin Heidelberg 2013

Published in the theme issue “Hydrogeology of Shallow Thermal Systems”

G. Schout · R. Schotting
Environmental Hydrogeology Group, Faculty of Geosciences,
Utrecht University, Budapestlaan 4, 3584 CD, Utrecht,
The Netherlands

B. Drijver (✉)
IF Technology, Velperweg 37, PO Box 605, 6800 AP, Arnhem,
The Netherlands
e-mail: b.drijver@iftechnology.nl
Tel.: +31-026-3535555
Fax: +31-026-3535599

M. Gutierrez-Neri
Department of Hydrology and Geo-Environmental Sciences,
Faculty of Earth and Life Sciences,
VU University Amsterdam, De Boelelaan 1085, 1081 HV,
Amsterdam, The Netherlands

High-temperature ATES (HT-ATES)

The advantage of HT-ATES (storage temperature $>60\text{ }^{\circ}\text{C}$) is that high temperatures can be used for direct heating. This can result in a significant improvement of the overall energy efficiency compared to low temperature ATES systems, which generally use heat pumps to upgrade the temperature level. HT-ATES applications can be of significant value, especially in connection with energy sources which are not controlled by immediate energy demand. Examples are waste residual heat (e.g. from power plants or industrial processes) and renewables like geothermal and solar heat. Another important advantage is that large temperature differences between the extracted and infiltrated water can be achieved, which means that the flow rate required for a specified heat demand is significantly lower than for low-temperature ATES. These advantages, combined with rising energy prices and an increasing focus on reduction of CO_2 -emissions have resulted in an increased interest in HT-ATES.

Despite the significant advantages, HT-ATES is hardly used in practice. Virtually all ATES systems in the Netherlands ($>99\%$) store low-temperature heat and cold in the range of $5\text{--}30\text{ }^{\circ}\text{C}$. There are several active ATES projects with storage temperatures in the range of $30\text{--}60\text{ }^{\circ}\text{C}$ (MT-ATES). Only two HT-ATES projects have been realized in The Netherlands and both have been closed. To the authors' knowledge, only two operational HT-ATES systems exist, both in Germany: the Reichstag Building in Berlin, where water is stored at $70\text{ }^{\circ}\text{C}$ (Sanner 1999; Kabus and Seibt 2000; Sanner et al. 2005; Kranz and Bartels 2010) and the HT-ATES system in Neubrandenburg where water is stored at $80\text{ }^{\circ}\text{C}$. The latter is a special case, however, as it uses two former deep geothermal wells for heat storage in a reservoir at $1,200\text{--}1,300\text{ m}$ depth with a native groundwater temperature of $55\text{ }^{\circ}\text{C}$ (Kabus et al. 2005; Kabus et al. 2009).

The main explanation for the limited number of projects is that HT-ATES is more complex as compared to low temperature ATES. In the 1980s, many technical problems arose in experimental and pilot plants (Sanner 1999). Issues that are important for the feasibility of HT-ATES are the risks of precipitation of minerals, corrosion of components in the groundwater system and low recovery efficiencies. The technical problems faced in cold storage and low temperature heat storage are less complex than those met in high temperature heat storage (Snijders 2000). In the period 1985–1995, much research was done to resolve these technical problems. This research demonstrated that the technical problems encountered can be solved and proven solutions are now available: water treatment methods to prevent precipitation of minerals (Sanner 1999; Drijver 2011), proper material selection to prevent corrosion and the use of low-permeability aquifers to reduce heat losses due to density-driven flow.

Other points of interest for HT-ATES are the increased impact on the groundwater composition and legal aspects. The impact on the groundwater composition is relatively large due to the large changes in temperature. The most

relevant issues are mobilization of organic carbon (Brons et al. 1991; Brons 1992; Bonte et al. 2011), potential scaling (Griffioen and Appelo 1993; Sanner 1999) and upconing of deeper groundwater caused by density-driven flow. Legal aspects that hinder the application of HT-ATES in the Netherlands are the maximum allowable storage temperature of $25\text{--}30\text{ }^{\circ}\text{C}$ and the requirement of an energy balance. Therefore, most MT and HT-ATES systems in the Netherlands are pilot-projects. The goal of these pilots is to gain more insight regarding the environmental impact of these types of systems, which can be used as input for policy makers when they are considering legislative changes. Options that have been mentioned are to allow the use of saltwater aquifers and deep aquifers to meet the demand for HT-ATES and make the related energy savings possible.

Recovery efficiency

One of the most important aspects controlling the feasibility of HT-ATES is the recovery efficiency. The recovery efficiency (ε) is defined here as the ratio between the recovered amount of energy and the stored amount of energy, with respect to the ambient temperature (T_a), when equal amounts of water are injected and produced.

$$\varepsilon = \frac{V_p \cdot C_w \cdot (\bar{T}_p - T_a)}{V_i \cdot C_w \cdot (T_i - T_a)} = \frac{\bar{T}_p - T_a}{T_i - T_a} \quad (1)$$

Where V_p and V_i are the produced and injected amounts of water [m^3], C_w is the volumetric heat capacity of water [$\text{J}/(\text{m}^3 \text{K})$], \bar{T}_p is the average temperature of the produced water [K] and T_i the injection temperature. In reality, production is usually stopped when the temperature of the produced water drops below a certain threshold temperature level known as the cut-off temperature. This has several interesting side effects. First and foremost, the efficiency will drop if the produced temperature drops below the cut-off temperature before the period with a net heat demand ends. If this is the case, more of the initially stored energy will be left behind in the aquifer, which can have implications for the recovery efficiency in subsequent years (as well as an environmental impact). In this study, the simplification was applied that any water that is recovered with a temperature above that of the ambient groundwater is useful.

The recovery efficiency of an ATES system is governed by the energy losses that occur as a result of a number of processes. Doughty et al. (1982) give an overview of these processes. They include thermal conduction, dispersion, regional groundwater flow and density-driven flow (also referred to as 'free convection' or 'buoyancy flow'). The relative contribution of these processes to the magnitude of the heat losses is determined by a number of operational properties (e.g. storage volume and storage temperature) as well as the properties

of the subsurface (e.g. the permeability and the thermal conductivity of the aquifer and confining layers).

Doughty et al. (1982) also present a graphical method to determine the recovery efficiency of an ATES system. Regional groundwater flow, heterogeneity and density-driven flow were not taken into account. For cases where the impact of groundwater flow becomes large, Doughty et al. (1982) refer to options to protect the storage region by using boundary wells. Aquifer heterogeneity influences the distribution of heat in the aquifer, but the influence on the recovery efficiency is small in most cases (Buscheck et al. 1983; Ferguson 2007; Caljé 2010). In case of strong heterogeneity (Sauty et al. 1978, 1982), or when the warm and cold wells are too close to each other (Sommer et al., Wageningen University, unpublished paper, 2013), the impact of heterogeneity can be significant.

However, the effect of density-driven flow has not been thoroughly addressed, while it is of particular relevance in a high-temperature application where a significant temperature contrast is present between the injected water and the ambient groundwater. This paper addresses the recovery efficiency of HT-ATES systems and includes the impact of density-driven flow.

Density-driven flow

Density-driven flow is caused by the difference in density between the injected water and the ambient groundwater. Due to the relatively low density, hot water that is stored has a tendency to flow in the upward direction in the aquifer. This causes the initially vertical thermal front (transition zone between the hot water and the surrounding cooler groundwater) to tilt. In the top part of the aquifer, hot water flows away from the well and, in the lower part of the aquifer, colder water flows towards the well screen. The rate of tilting of the thermal front is given by the characteristic tilting time, t_0 (Hellström and Tsang 1988a):

$$t_0 = \frac{H}{\sqrt{k_a^h \cdot k_a^v}} \cdot \frac{C_a}{C_w} \cdot \frac{\pi^2 \cdot (\mu_a + \mu_i)}{32 \cdot G \cdot (\rho_a - \rho_i) \cdot g} \quad (2)$$

where H is the aquifer thickness [m], k_a^h and k_a^v are the horizontal and vertical aquifer permeability [m^2], C_a and C_w are the volumetric heat capacities of the (water saturated) aquifer and of water [$\text{J}/(\text{m}^3 \text{K})$], μ_a and μ_i are the dynamic viscosities of the ambient and the injected water [$\text{kg}/(\text{m}\cdot\text{s})$], ρ_a and ρ_i are the densities [kg/m^3] G is Catalan's constant and g is the acceleration of gravity (9.81 m/s^2) (≈ 0.916). According to Doughty et al. (1982), the buoyancy tilting of an initially vertical front during a time t_0 is about 60° . If the time of the cycle is smaller than t_0 , the tilting is expected to be moderate and, thus, its influence on the recovery efficiency is relatively small. The characteristic tilting time (t_0) was derived by Hellström et al. (1979) for the plane case, but the magnitude does not change significantly for the radial case (Doughty et al. 1982). If the thermal front is diffuse

rather than sharp, the tilting rate is slightly lowered. Furthermore, as the thermal front tilts, the flow resistance in the hot part of the aquifer is reduced because of the lower viscosity of hot water. Forced convection, then, gives an increase of the tilting rate during injection periods and a decrease during production periods for hot water storage (Doughty et al. 1982). Due to the tilted front, the zone of reduced flow resistance extends further from the well in the top part of the aquifer. As a consequence, the contribution of well screen sections in the top part of the aquifer to the total flow rate is relatively high. Because the angle of tilt is larger during production than during injection, this tends to decrease the impact on the recovery efficiency.

The characteristic tilting time is mainly influenced by the temperature (which determines μ and ρ) and the horizontal and vertical permeability. This means that thermal losses due to tilting can be minimized by reducing the temperature difference (i.e. choosing a lower storage temperature or a deeper aquifer with a higher ambient temperature), and/or by selecting a low permeability aquifer. The characteristic tilting time is also linearly dependent on the aquifer thickness, suggesting the selection of thick aquifers. However, because the thermal radius (the horizontal extent of the approximately cylindrically shaped storage volume, defined as $\sqrt{(V_i C_w / \pi H C_a)}$) is more or less fixed, the impact of the same tilting angle on the recovery efficiency is approximately proportional to the thickness. Doubling the aquifer thickness, thus, results in two effects that more or less compensate each other: a reduction of the tilting angle by 50 % and an increase of the impact of the same tilting angle by a factor two. The influence of the aquifer thickness on the percentage heat loss due to density-driven flow is therefore expected to be limited. Nevertheless, the aquifer thickness can be important for the heat losses through conduction, because it controls the surface area to volume ratio of the storage plume (e.g. Doughty et al. 1982).

Rayleigh number

Gutierrez-Neri et al. (2011) conducted a numerical study that evaluated the recovery efficiency of HT-ATES systems. Although the number of simulated scenarios was limited, a correlation was found between the calculated recovery efficiencies and the Rayleigh number (Ra). The dimensionless Ra indicates the relative strength of heat transfer through conduction and free convection (Nield and Bejan 1999). It is defined as:

$$Ra = \frac{\alpha \cdot \rho \cdot g \cdot H \cdot C_a \cdot k_a^v \cdot \Delta T}{\mu \cdot \lambda_a} \quad (3)$$

where α is the coefficient of thermal expansion of water [$1/\text{K}$], λ_a [m^2/s], ΔT is the temperature difference between the injected and ambient groundwater [K], μ is the dynamic

viscosity of water [kg/(m·s)] and λ_a is the horizontal aquifer thermal conductivity [W/(m² K)]. The density and the viscosity have to be assessed at the “average system temperature”, T_m :

$$T_m = \frac{T_{\min} + T_{\max}}{2} = \frac{T_a + T_i}{2} \quad (4)$$

where T_a is the ambient groundwater temperature [K] and T_i the temperature of the injected water [K]. The onset of free convection in a porous medium layer bounded in the top and base by impermeable, perfectly conducting layers has been investigated by a number of authors (e.g. Lapwood 1948; Katto and Masuoka 1967; Nield 1975; Tan and Sam 1999). According to Lapwood, the criterion for the appearance of free convection can be written in terms of a critical Ra, Ra_c , found to be approximately equal to $4\pi^2$. This means that if the system's $Ra < Ra_c$, the dominant heat transfer process will be heat conduction. When the system's $Ra > Ra_c$, free convection will be the dominant process.

Figure 1 shows the correlation found by Gutierrez-Neri et al. (2011). It can be seen that recovery efficiency is strongly affected by free convection. Below the Ra_c , heat losses due to conduction will be relatively small compared to convection-induced losses. However, as the Ra increases, the impact of free convection on the recovery efficiency increases significantly.

In order to develop a functional relationship that reliably predicts the recovery efficiency of HT-ATES, the analysis presented in Gutierrez-Neri et al. (2011) was replicated and extended. A larger number of HT-ATES scenarios were modeled and a relationship was sought between the Ra and the recovery efficiency that fits the entire data set. The resulting function should allow for quick estimates of the potential for HT-ATES at specific sites and to assist in optimizing system configurations.

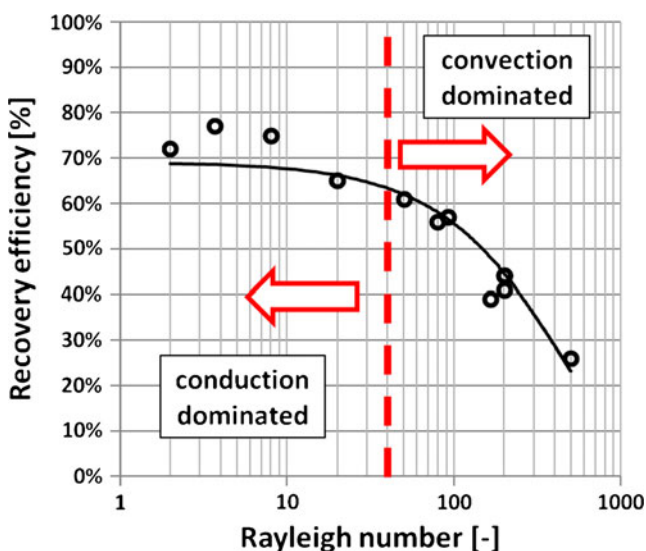


Fig. 1 Relation between the Ra and the recovery efficiency as found by Gutierrez-Neri et al. (2011). The vertical dotted line represents the critical Ra

Methods

HT-ATES systems were modeled using HstWin-2D, a numerical code specially developed for heat and solute transport in porous media. The code takes into account the dependency of both viscosity and density on temperature and concentration changes and has been previously validated to a number of analytical solutions (Kipp 1987).

A two-dimensional (2-D) radial configuration was used to model the expected symmetrical effects around the storage/recovery well. As a consequence, the influence of regional groundwater flow is neglected. In most cases, this assumption will prove to be acceptable, since (1) the hydraulic gradient in the relatively deep aquifers where HT-ATES is applied is usually low and (2) the permeability of the selected aquifer will be low (to minimize density-driven flow). Another limitation is that it is not possible to model other wells: a single injection/production well is assumed. The impact of the “cold” well is therefore not included and is assumed to be insignificant.

All model simulations are variations on a single base-case, which was chosen equal to the base case that was used in the work of Buscheck (1984), allowing for a comparison of the results as a means of model validation. Buscheck's model results were in turn validated using data from a large field experiment at the Auburn University in Mobile, Alabama (USA), and have been proven to be accurate (Tsang et al. 1981; Buscheck 1984). The base case assumes heat storage through a fully penetrating injection/production well in a horizontal aquifer of 21 m thickness that is confined by two clay layers of 9 m thickness (Fig. 2). All three of the modeled layers are assumed to be homogeneous. The aquifer permeabilities in the horizontal (k_a^h) and vertical direction (k_a^v) are 15 and 1.5 Darcy (D), respectively. The confining layers are practically impermeable ($k_c/k_a^h=10^{-5}$). The thermal conductivity and volumetric heat capacity (λ_a and $\rho_a C_a$) for both the aquifer and confining layers are 2.56 W/(m·K) and 1.81 MJ/(m³·K). One cycle consists of four periods of 90 days. During the injection period (t_i), a volume of 55,000 m³ (V_i) of water with a constant temperature of 90 °C (T_i) is injected into the aquifer with a constant flow rate (Q_i). The ambient groundwater temperature (T_a) has a constant value of 20 °C. After the storage period (t_s), the same volume (V_p) is produced in the production period (t_p), again with a constant flow rate (Q_p). The cycle is finalized by a rest period (t_r). A full list of base-case parameter values can be found in Tables 1 and 2.

The model domain has a thickness of 39 m and a radial extent of 1,000 m. A series of preliminary runs were carried out to find the right combination of grid dimensions and maximum simulation time step. Appropriate results were obtained for square grid elements with $dr=dz=1$ m within the zone of the thermal radius (R_{th}), then a series of grid cells with $dr=0.5$ m, followed by a logarithmic increase in the grid spacing. The vertical grid spacing at the transition between the aquifer and confining layers was also reduced to 0.5 m. The maximum time-step length was set to 0.5 days. A constant

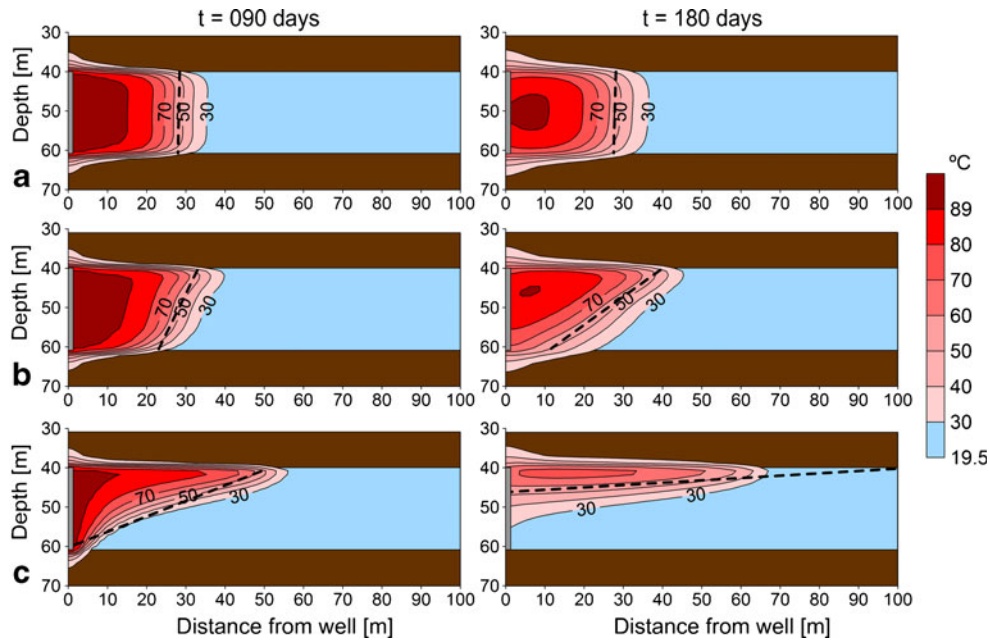


Fig. 2 Contour plots of the calculated groundwater temperatures at the end of the injection period ($t=90$ days; left panel) and at the end of the storage period ($t=180$ days; right panel) for scenarios with different values for the aquifer permeability. With **a** $k_a^v=25$ D and $k_a^h=0.1$ D; **b** $k_a^h=15$ D and $k_a^v=1.5$ D; and **c** $k_a^h=50$ D and $k_a^v=25$ D. For all scenarios, $T_i=90$ °C, $T_a=20$ °C and $V_i=55,000$ m³. The angle of tilt is measured as the angle of the average system temperature contour (55 °C) with the vertical

temperature boundary condition was assumed at the top and bottom of the model. The vertical boundary at $r=1,000$ m was modeled as a constant temperature and pressure boundary.

Calculated recovery efficiencies for this setup were found to stabilize after more or less 4 years. This is in agreement with the findings of Gutierrez-Neri et al. (2011), where recovery efficiencies were also found to stabilize after around 4 years. The recovery efficiency in the fourth year was therefore selected for further analysis.

Results

Model validation

For a number of cases it was possible to compare the results with those of Buscheck (1984) as a means of validation. As Buscheck (1984) mainly focuses on the angles of tilt and relatively few recovery efficiencies are given, the model results for the angle of tilt were compared for 14 scenarios (at the end of the injection

period and the end of the storage period of the first year). The angles of tilt of a number of scenarios at two different points in time can be observed in Fig. 2. A dotted line in Fig. 2 represents an angle of tilt. These are determined for the contour line of the ‘average system temperature’ (T_m). The average difference of the angles of tilt calculated in this study with respect to those calculated by Buscheck for the same scenarios was found to be 2.83° (Table 3). The present model results are thus in good agreement with the results found by Buscheck (1984). In combination with the fact that HSTWin-2D is a validated program for heat transport simulations, this gives confidence in the validity of the numerically predicted recovery efficiencies.

Sensitivity analysis

Table 4 shows the recovery efficiency of a number of scenarios where one or two parameters were varied with respect to the base-case. It shows that variations in permeability (both horizontal and vertical), injection temperature and injection volume have the greatest

Table 1 Hydrogeological parameter values as used in the base case

Parameter	Aquifer		Confining layers		Units
	Symbol	Value	Symbol	Value	
Horizontal permeability	k_a^h	$15 \cdot 10^{-12}$	k_c^h	$15 \cdot 10^{-17}$	m ²
Vertical permeability	k_a^v	$1.5 \cdot 10^{-12}$	k_c^v	$1.5 \cdot 10^{-17}$	m ²
Thickness	H	21	D	9	m
Porosity	n_a	0.25	n_c	0.35	–
Thermal conductivity	λ_a	2.56	λ_c	2.56	W/(m·K)
Volumetric heat capacity	C_a	$1.81 \cdot 10^6$	C_c	$1.81 \cdot 10^6$	J/(m ³ ·K)
Ambient temperature	T_a	20	T_a	20	°C
Longitudinal dispersivity	d_{II}	0.7	–	–	m

Table 2 Operational parameter values as used in the base case

Parameter	Injection and production		Storage and rest		Units
	Symbol	Value	Symbol	Value	
Pumped volume	$V_i=V_p$	55,000	–	–	m^3
Flow rate	$Q_i=Q_p$	25.5	–	–	m^3/h
Injection temperature	T_i	90	–	–	$^{\circ}C$
Duration	$t_i=t_p$	90	$t_s=t_r$	90	Days

impact. The change in recovery efficiency due to variations in thermal conductivity, longitudinal dispersivity or permeability of the confining layer is much smaller. The change in recovery efficiency due to changes in aquifer thickness seems to be small as well; however, it is partly disguised, as the thermal radius was kept equal in these scenarios, which means that the injected and produced volumes were also changed. A simulation was also performed with an injection period and production period of 180 days (while the total injected volume was kept equal). The result suggests that different (symmetrical) time schemes with an annual cycle have a relatively small influence on the recovery efficiency.

Correlation to the Rayleigh number

In Fig. 3, the model results for the set of scenarios with an aquifer thickness of 21 m are plotted against the Ra. A summary of these scenarios' properties, as well as those of all other modeled scenarios, can be found in Table 5. The graph shows their Ra on the x-axis and their recovery efficiency on the y-axis. The best fit through this scatterplot is an exponential relationship with a relatively poor correlation coefficient ($R^2=0.49$). Striking in Fig. 3 is that many of the plotted scenarios have the same Ra, but different recovery efficiencies. This implies that a number

of parameters that lead to significant differences in the recovery efficiency do not affect the Ra.

To improve this relation, these missing parameters were included in an adjusted version of the Ra. Comparing the most influential parameters from Table 4 with the parameters in the Ra reveals the parameters that are missing. They are the horizontal aquifer permeability (k_a^h) and the injection volume (V_i). The importance of the horizontal aquifer permeability is apparent from the formula for the characteristic tilting time, which indicates the importance of heat losses as a consequence of density-driven flow. In accordance with the formula for the characteristic tilting time, k_a^v was replaced by $\sqrt{(k_a^h k_a^v)}$. Since the injection volume for a given aquifer height (already included in the Ra) is inversely proportional to the aspect ratio, H/R_{th} , of the system (proportional to R_{th}/H), the Ra was divided by R_{th}/H (which is equivalent to multiplication with the aspect ratio), giving:

$$Ra^* = \frac{\alpha \cdot \rho \cdot g \cdot H^2 \cdot C_a \cdot \sqrt{k_a^v k_a^h} \cdot \Delta T}{\mu \cdot \lambda_a \cdot R_{th}} \quad (5)$$

In Table 4, the impact of the heat capacity and thermal conductivity on the recovery efficiency was shown to be

Table 3 Difference in the angle of tilt ($\Delta\alpha$) as derived from model calculations (α_{model}) in comparison to the values given by Buscheck (1984) (α_{lit}). Average deviation for the study = 2.83°. All units in degrees (°). DDarcy

Scenario ^a	Time: 90 days			Time: 180 days		
	α_{lit}	α_{model}	$\Delta\alpha$	α_{lit}	α_{model}	$\Delta\alpha$
AI90	46.1	49	2.9	64.6	65.5	0.9
AT90	40.3	43	2.7	65.5	65.5	0
AL90	36	38	2	63.9	64.5	0.6
AI55	16.6	13	3.6	32.2	34	1.8
AT55	13.9	14	0.1	23	34	11
AL55	13	14	1	24	29	5
BI90	71	75.5	4.5	82.8	84.5	1.7
BT90	68	75	7	80.9	85	4.1
BL90	66.4	73.5	7.1	81.7	85	3.3
BI55	44	47	3	64.5	66.5	2
BT55	39.2	38	1.2	64.9	66	1.1
BL55	35	33	2	64.1	64.5	0.4
CI55	71.3	68	3.3	83.7	84	0.3
CT55	67.1	66	1.1	80.8	84	3.2
CL55	67	62	5	81	84	3

^a The first and second letters of the scenario code indicate variations in the properties of the aquifer (*A*, *B* and *C*) and the confining layers (*I*, *T* and *L*) and the number at the end indicates the injection temperature (55 or 90 °C):

A: $k_a^h=15$ D and $k_a^v=1.5$ D; *B*: $k_a^h=52$ D and $k_a^v=5.2$ D; *C*: $k_a^h=175$ D and $k_a^v=17.5$ D

I: $k_c^h=15 \cdot 10^{-5}$ D, $k_c^v=1.5 \cdot 10^{-5}$ D and $\lambda_c=0$ W/(m·K); *T*: $k_c^h=15 \cdot 10^{-5}$ D, $k_c^v=1.5 \cdot 10^{-5}$ D and $\lambda_c=2.56$ W;

L: $k_c^h=15 \cdot 10^{-1}$ D, $k_c^v=1.5 \cdot 10^{-1}$ D and $\lambda_c=2.56$ W/(m·K)

Table 4 Summary of calculated recovery efficiencies and the input values analyzed in the sensitivity analyses. Shown are the recovery efficiencies for each of the scenarios in year 4 (ε), as well as the difference in recovery efficiency compared to the base case ($\Delta\varepsilon$). Values given in *italics* represent variations on the base case

Variation	ε [%] ^a	$\Delta\varepsilon$ [%] ^a	k_a^h [D] ^b	k_a^v [D] ^b	T_i [°C]	V_i [m ³]	H [m]	R_{th} [m]	λ_a [W/(m·K)]	d_{II} [m]	k_c^h [D] ^b	k_c^v [D] ^b	C_a [J/m ³ ·°C]	t_i [d] ^c V
Base case	64	–	15	1.5	90	55,000	21	43.5	2.56	0.7	$1.5 \cdot 10^{-4}$	$1.5 \cdot 10^{-5}$	$1.81 \cdot 10^6$	90
k	43	–21	52	5.2	90	55,000	21	43.5	2.56	0.7	$5.2 \cdot 10^{-4}$	$5.2 \cdot 10^{-5}$	$1.81 \cdot 10^6$	90
k_a^v	59	–5	15	5	90	55,000	21	43.5	2.56	0.7	$1.5 \cdot 10^{-4}$	$1.5 \cdot 10^{-5}$	$1.81 \cdot 10^6$	90
k_a^v	57	–7	15	15	90	55,000	21	43.5	2.56	0.7	$1.5 \cdot 10^{-4}$	$1.5 \cdot 10^{-5}$	$1.81 \cdot 10^6$	90
T_i	74	+10	15	1.5	55	55,000	21	43.5	2.56	0.7	$1.5 \cdot 10^{-4}$	$1.5 \cdot 10^{-5}$	$1.81 \cdot 10^6$	90
V_i	74	+10	15	1.5	90	165,000	21	75.3	2.56	0.7	$1.5 \cdot 10^{-4}$	$1.5 \cdot 10^{-5}$	$1.81 \cdot 10^6$	90
V_i	52	–12	15	1.5	90	18,300	21	25.2	2.56	0.7	$1.5 \cdot 10^{-4}$	$1.5 \cdot 10^{-5}$	$1.81 \cdot 10^6$	90
H	63	–1	15	1.5	90	27,500	10	43.5	2.56	0.7	$1.5 \cdot 10^{-4}$	$1.5 \cdot 10^{-5}$	$1.81 \cdot 10^6$	90
H	65	+1	15	1.5	90	110,000	42	43.5	2.56	0.7	$1.5 \cdot 10^{-4}$	$1.5 \cdot 10^{-5}$	$1.81 \cdot 10^6$	90
$9\lambda_a$	67	+3	15	1.5	90	55,000	21	43.5	0	0.7	$1.5 \cdot 10^{-4}$	$1.5 \cdot 10^{-5}$	$1.81 \cdot 10^6$	90
d_{II}	64	0	15	1.5	90	55,000	21	43.5	2.56	0	$1.5 \cdot 10^{-4}$	$1.5 \cdot 10^{-5}$	$1.81 \cdot 10^6$	90
k_c	64	0	15	1.5	90	55,000	21	43.5	2.56	0.7	$1.5 \cdot 10^{-2}$	$1.5 \cdot 10^{-3}$	$1.81 \cdot 10^6$	90
k_c	61	–3	15	1.5	90	55,000	21	43.5	2.56	0.7	1.5	$1.5 \cdot 10^{-1}$	$1.81 \cdot 10^6$	90
C_a	65	+1	15	1.5	90	55,000	21	37.9	2.56	0.7	$1.5 \cdot 10^{-4}$	$1.5 \cdot 10^{-5}$	$2.50 \cdot 10^6$	90
C_a	66	+2	15	1.5	90	55,000	21	34.6	2.56	0.7	$1.5 \cdot 10^{-4}$	$1.5 \cdot 10^{-5}$	$3.00 \cdot 10^6$	90
t_i	66	+2	15	1.5	90	55,000	21	43.5	2.56	0.7	$1.5 \cdot 10^{-4}$	$1.5 \cdot 10^{-5}$	$1.81 \cdot 10^6$	180

^aThe recovery efficiency is given for the fourth year

^bPermeability values are given in Darcy (D). 1 D is equal to 10^{-12} m²

^cIn the base case, one cycle consists of a 90-day injection and production period and two 90-day rest periods. In this variation, one cycle consists of a 180-day injection and a 180-day production period

insignificant within the typically occurring range of values. However, in Eq. 5, these parameters are equally important to the Ra as, e.g. the permeability and injection temperature, which have been shown to exert a much greater influence on the recovery efficiency. Both the heat capacity and thermal conductivity were therefore converted to constants assuming the values shown in the base case. Furthermore, R_{th} is replaced by $\sqrt{(V_i C_w / \pi H C_a)}$ and the equation is simplified. Together with all other constants that are included in the

modified Ra, this results in a simplified formula with one constant replacing α_f , g , C_w , C_a , λ_a and π , giving:

$$Ra^* = 1634 \cdot \frac{\rho \cdot H^{2.5} \cdot \sqrt{k_a^v \cdot k_a^h} \cdot \Delta T}{\mu \cdot \sqrt{V_i}} \tag{6}$$

The correlation between this modified Ra and the recovery efficiency in the fourth year is shown in Fig. 4 and has improved strongly compared to Fig. 3 (correlation coefficient increased to 0.96).

To check the general applicability of Eq. 6, a series of extra scenarios was simulated for a number of different aquifer thicknesses. In this way, the data set of the recovery efficiencies was extended to 78 scenarios (Table 5). Figure 5 shows the resulting scatter plots, with each aquifer thickness represented by a different color. It appears that for each aquifer thickness, the curves of their exponential functions have to be shifted to obtain an appropriate fit. To get one equation capable of predicting the recovery efficiency for all scenarios, further adjustments are necessary. In general the exponential functions that were found take the form of:

$$\varepsilon = A \cdot e^{(B \cdot Ra^*)} \tag{7}$$

For every set of scenarios with the same aquifer thickness, the values of A and B are constant, but A and B differ for scenarios with different aquifer thicknesses; therefore, relations were sought for A and B as a function

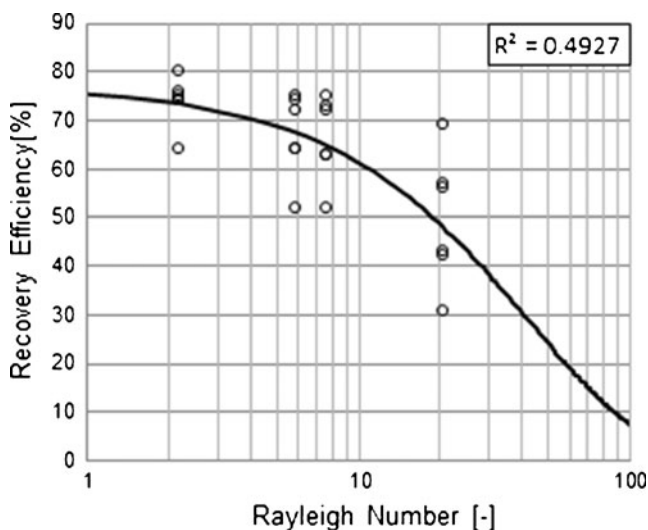


Fig. 3 The correlation between the Ra (Eq. 3) and the recovery efficiency in the fourth year of all modeled scenarios with an aquifer thickness of 21 m. The exponential trend line in this figure is described by $\varepsilon = 77.318e^{(-0.023 \cdot Ra)}$

Table 5 Summary of the characteristics and recovery efficiencies of the modeled scenarios that form the database. Values given in *italics* represent variations on the base case

Scenario	V_i [m ³]	R_{th} [m]	R_{th}/H	T_i [°C]	k_a^v [D]	k_a^h [D]	k_c^v [D]	k_c^h [D]	ϵ_{10} [%]	ϵ_{21} [%]	ϵ_{42} [%]	ϵ_{63} [%]
AT90	55,000	43.46	2.07	90	1.5	15	$1.5 \cdot 10^{-4}$	$1.5 \cdot 10^{-5}$	63	64	65	68
AB90	55,000	43.46	2.07	90	1.5	15	$1.5 \cdot 10^{-2}$	$1.5 \cdot 10^{-3}$	63	64	65	68
AB55	55,000	43.46	2.07	55	1.5	15	$1.5 \cdot 10^{-2}$	$1.5 \cdot 10^{-3}$	67	74	77	79
AT55	55,000	43.46	2.07	55	1.5	15	$1.5 \cdot 10^{-4}$	$1.5 \cdot 10^{-5}$	67	74	77	79
BB90	55,000	43.46	2.07	90	5.2	52	$1.5 \cdot 10^{-2}$	$1.5 \cdot 10^{-3}$	49	42	40	40
BT90	55,000	43.46	2.07	90	5.2	52	$1.5 \cdot 10^{-4}$	$1.5 \cdot 10^{-5}$	49	43	39	40
BB55	55,000	43.46	2.07	55	5.2	52	$1.5 \cdot 10^{-2}$	$1.5 \cdot 10^{-3}$	63	63	64	67
BT55	55,000	43.46	2.07	55	5.2	52	$1.5 \cdot 10^{-4}$	$1.5 \cdot 10^{-5}$	63	63	64	67
AT90V3	165,000	75.27	3.58	90	1.5	15	$1.5 \cdot 10^{-4}$	$1.5 \cdot 10^{-5}$	71	74	74	75
BT90V3	165,000	75.27	3.58	90	5.2	52	$1.5 \cdot 10^{-4}$	$1.5 \cdot 10^{-5}$	63	57	52	51
AT55V3	165,000	75.27	3.58	55	1.5	15	$1.5 \cdot 10^{-4}$	$1.5 \cdot 10^{-5}$	73	80	83	85
BT55V3 ^a	165,000	75.27	3.58	55	5.2	52	$1.5 \cdot 10^{-4}$	$1.5 \cdot 10^{-5}$	–	73	–	–
AT90Vs	18,500	25.20	1.20	90	1.5	15	$1.5 \cdot 10^{-4}$	$1.5 \cdot 10^{-5}$	50	52	56	60
BT90Vs	18,500	25.20	1.20	90	5.2	52	$1.5 \cdot 10^{-4}$	$1.5 \cdot 10^{-5}$	36	31	30	33
AT55Vs	18,500	25.20	1.20	55	1.5	15	$1.5 \cdot 10^{-4}$	$1.5 \cdot 10^{-5}$	57	64	68	71
BT55Vs ^a	18,500	25.20	1.20	55	5.2	52	$1.5 \cdot 10^{-4}$	$1.5 \cdot 10^{-5}$	–	52	–	–
AT90r3	55,000	43.46	2.07	90	1.5	4.5	$1.5 \cdot 10^{-4}$	$1.5 \cdot 10^{-5}$	67	72	73	74
AT90r1	55,000	43.46	2.07	90	1.5	1.5	$1.5 \cdot 10^{-4}$	$1.5 \cdot 10^{-5}$	68	75	77	78
BT90r3	55,000	43.46	2.07	90	5.2	15.6	$1.5 \cdot 10^{-4}$	$1.5 \cdot 10^{-5}$	61	56	53	52
BT90r1	55,000	43.46	2.07	90	5.2	5.2	$1.5 \cdot 10^{-4}$	$1.5 \cdot 10^{-5}$	66	69	66	56
AT55r3 ^a	55,000	43.46	2.07	55	1.5	4.5	$1.5 \cdot 10^{-4}$	$1.5 \cdot 10^{-5}$	–	75	–	–
AT55r1 ^a	55,000	43.46	2.07	55	1.5	1.5	$1.5 \cdot 10^{-4}$	$1.5 \cdot 10^{-5}$	–	76	–	–
BT55r3 ^a	55,000	43.46	2.07	55	5.2	15.6	$1.5 \cdot 10^{-4}$	$1.5 \cdot 10^{-5}$	–	72	–	–
BT55r1 ^a	55,000	43.46	2.07	55	5.2	5.2	$1.5 \cdot 10^{-4}$	$1.5 \cdot 10^{-5}$	–	75	–	–

^a Scenarios were only modeled with an aquifer thickness of 21 m; all other scenarios were modeled with all selected aquifer thicknesses (10, 21, 42 and 63 m). All other properties are equal to those of the base case as shown in Tables 1 and 2

of the aquifer thickness. Through curve-fitting the following relation was found for A :

$$A = 0.82 - \frac{1.70}{H^{1.2}} \tag{8}$$

For B , two relations were needed. Equation (9) is valid when the aquifer thickness is between 10 and 60 m and Eq. (10) between 60 and 200 m:

$$B_1 = -\frac{1.2}{H^{1.35}} + 2.2 \cdot 10^{-3} \tag{9}$$

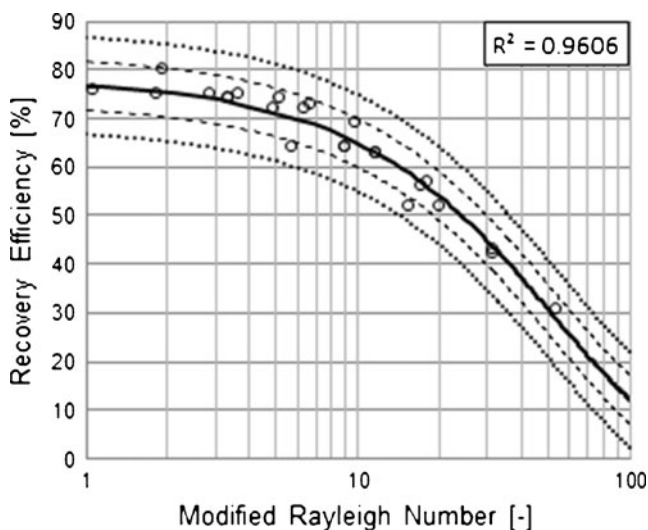


Fig. 4 The correlation between the modified Ra (Eq. 6) and the recovery efficiency in the fourth year of all modeled scenarios with an aquifer thickness of 21 m. The *dashed and dotted lines* show the $\pm 5\%$ and $\pm 10\%$ zones, respectively

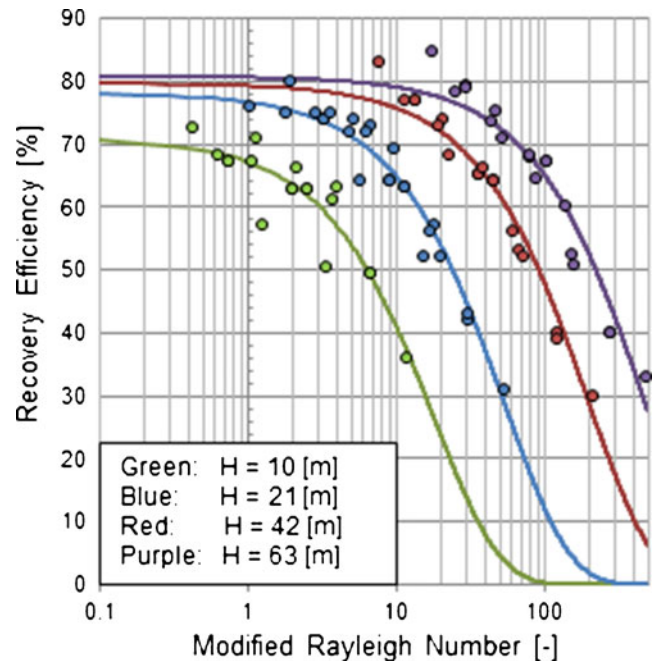


Fig. 5 The correlation between the modified Ra (Eq. 6) and the recovery efficiency in the fourth year for all modeled scenarios. *Green, blue, red and purple circles* are the data points and the exponential trend lines corresponding with aquifer thicknesses of respectively 10, 21, 42 and 63 m.

$$\begin{aligned} \epsilon_{(H=10)} &= 70.915e^{(-0.055 \cdot Ra^*)}, R^2 = 0.8646; \epsilon_{(H=21)} = 78.114e^{(-0.019 \cdot Ra^*)}, R^2 = 0.9606; \\ \epsilon_{(H=42)} &= 79.671e^{(-0.005 \cdot Ra^*)}, R^2 = 0.9639; \epsilon_{(H=63)} = 80.776e^{(-0.002 \cdot Ra^*)}, R^2 = 0.9273 \end{aligned}$$

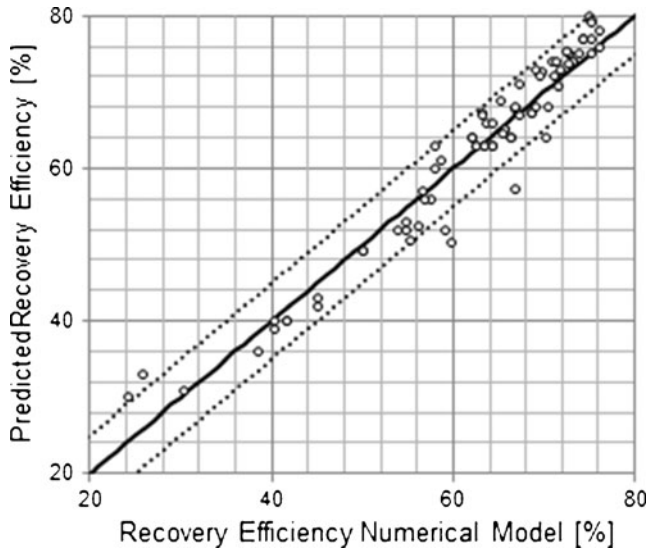


Fig. 6 The accuracy of the ‘Rayleigh method’. Shown are the recovery efficiencies predicted by Eqs. (11) and (12), plotted against the numerically obtained recovery efficiencies. The *solid black line* shows the 1 to 1 (ideal) relationship and the *dotted lines* show the ±5 % zone. Nearly all computed scenarios can be observed to be predicted within 5 % of the numerically modeled recovery efficiency

$$B_2 = \frac{-2.7}{H^{1.7}} \tag{10}$$

Ultimately this yields two Eqs. (11) and (12) which are capable of predicting the recovery efficiency of HT-ATES for aquifer thicknesses of 10 m up to 200 m:

$$\text{When } 10 < H < 60 \text{ [m]} \quad \varepsilon = \left(0.82 - \frac{1.70}{H^{1.2}}\right) \cdot e^{\left(-\frac{12}{H^{1.35}} + 2.2 \cdot 10^{-3}\right) \cdot Ra^*} \tag{11}$$

$$\text{When } 60 < H < 200 \text{ [m]} \quad \varepsilon = \left(0.82 - \frac{1.70}{H^{1.2}}\right) \cdot e^{\left(\frac{-2.7}{H^{1.7}}\right) \cdot Ra^*} \tag{12}$$

Figure 6 shows the accuracy of the numerically predicted efficiencies using the preceding equations, or ‘Rayleigh method’. The average (absolute) error in the predicted recovery efficiencies with respect to the numerically modeled values is 2.79 %.

Discussion

The developed method for estimating the recovery efficiency of HT-ATES has been shown to be accurate within a few percentage points. The proposed formulas can be used either by inserting the required variables directly or with, for example, a contour plot such as the one shown in Fig. 7. The method is therefore useful to get a quick impression of the potential for HT-ATES at specific sites. Since only the most basic information about the subsurface is required (aquifer permeability, aquifer thickness and ambient temperature), the most suitable aquifers (from the recovery efficiency point of view) can easily be selected. Furthermore, it can be used for a sensitivity analysis, giving insight into possibilities for optimizing an envisioned HT-ATES system.

An additional factor that is of major importance for the recovery efficiency of HT-ATES is the cut-off temperature. As mentioned in the introduction, the assumption was made in this study that any water that is recovered with a temperature above that of the ambient groundwater is useful. In reality, production is usually stopped when temperatures drop below a certain threshold at which it is no longer useful for the above ground application. If this is the case, the recovery efficiency will be lower than the

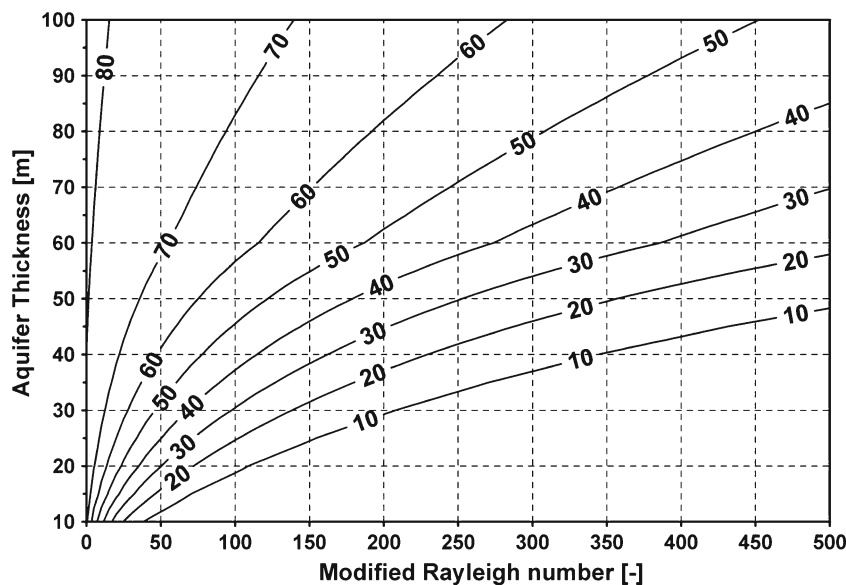


Fig. 7 Recovery efficiency [%] as a function of the modified Ra and the aquifer thickness (H). Above and below H=60 m, the appropriate formulas have been applied: Eq. (11) below H=60 m and Eq. (12) above H=60 m

equations predict. To incorporate the cut-off temperature in the proposed method, further research is therefore required. For the exact effects of a cut-off temperature on the recovery efficiency, detailed and site-specific numerical simulation will remain necessary.

Options to optimize the recovery efficiency and/or the extraction temperature have also been suggested and can be useful in practice. Injecting an extra amount of hot water before or during the first cycle can help to overcome the problem of relatively low recovery efficiencies in the first years (Sauty et al. 1982). Surrounding the hot wells with a number of relatively warm wells may help to increase the apparent ambient temperature. Using only part of the screen for injection (lower part) and/or extraction (upper part) can also help (Buscheck et al. 1983; Buscheck 1984), especially when a cut-off temperature is the limiting factor. Most research into such techniques has been conducted in the field of ASR (aquifer storage and recovery), where the problem of density-driven flow is the consequence of storage of (relatively low density) freshwater in brackish or saltwater aquifers (e.g. Ward et al. 2007). Additional research could focus on the suitability of such techniques for optimization of HT-ATES performance.

Conclusions

Heat loss due to density-driven flow is one of the key factors that determine the recovery efficiency of HT-ATES systems. Because the R_a is a measure of the relative strength of heat transport by density-driven flow compared to heat conduction, it can be used as an indicator for the recovery efficiency. A modified R_a is introduced that gives a good correlation with the recovery efficiency of HT-ATES systems in the 4th year, when the recovery efficiency more or less stabilizes (Eq. 5). The modified R_a is only dependent on a limited number of key parameters: the aquifer thickness, horizontal and vertical aquifer permeability, injection volume, injection temperature and ambient temperature. Two exponential relationships were derived (Eqs. 11 and 12) for two aquifer thickness intervals that accurately reproduce all numerically modeled scenarios with an average error of less than 3 %. The presented method has only been tested within the range of values that was used and is expected to be inaccurate in extreme scenarios such as very large or small injection volumes and/or highly heterogeneous aquifers. The presented method has proven to be effective at temperatures higher than 50 °C (30 °C higher than the ambient groundwater temperature that was assumed). An important assumption is that the injected and produced amounts of water are equal, which means that the analytical solutions are not valid when a cut-off temperature limits the (useful) amount of water that can be produced.

The method described can be useful when a HT-ATES system is considered or in the design phase. It can be used to select the best aquifer and/or location for HT-ATES and

gives a first estimate of the recovery efficiency that can be expected. In this way, the economic feasibility of HT-ATES can be assessed without running numerical simulations to predict the recovery efficiency. Later on, it may still be necessary to do detailed simulations, for instance to consider specific features of a given site, specific characteristics related to the predicted use of the system or methods to optimize the recovery efficiency.

Acknowledgements We thank the Dutch Foundation on Soil Knowledge Development and Transfer (SKB) for funding this research, Thomas Buscheck for making available his valuable thesis and Christine Doughty and Jörn Bartels for their critical reviews of our work.

References

- Bonte M, Visser P, Kooi H, van Breukelen B, Claas J, Chacón Rovati V and Stuyfzand P (2011) Effects of aquifer thermal energy storage on groundwater quality elucidated by field and laboratory investigations. First Dutch Geothermal Congress, Utrecht, The Netherlands, October 2011
- Brons HJ (1992) Biogeochemical aspects of aquifer thermal energy storage. PhD Thesis, Wageningen University, The Netherlands, 127 pp
- Brons HJ, Griffioen J, Appelo CAJ, Zehnder AJB (1991) (Bio)geochemical aquifer material from a thermal-energy storage site. *Water Res* 25(6):729–736
- Buscheck TA (1984) The hydrothermal analysis of aquifer thermal energy storage. PhD Thesis, University of California, Berkeley, USA
- Buscheck TA, Doughty C, Tsang CF (1983) Prediction and analysis of a field experiment on a multi-layered aquifer thermal energy storage system with strong buoyancy flow. *Water Resour Res* 19(5):1307–1315
- Caljé, RJ (2011) Future use of Aquifer Thermal Energy Storage below the historic centre of Amsterdam. Master thesis, Delft University of Technology
- Doughty C, Hellström G, Tsang CF, Claesson J (1982) A dimensionless parameter approach to the thermal behaviour of an aquifer thermal energy storage system. *Water Resour Res* 18(3):571–587
- Drijver BC (2011) High temperature aquifer thermal energy storage (HT-ATES): water treatment in practice. First Dutch Geothermal Congress, Utrecht, The Netherlands, October 2011
- Ferguson G (2007) Heterogeneity and thermal modeling of groundwater. *Groundwater* 45(4):485–490
- Griffioen J, Appelo CAJ (1993) Nature and extent of carbonate precipitation during aquifer thermal energy storage. *Appl Geochem* 8(2):161–176
- Gutierrez-Neri M, Buik N, Drijver B, Godschalk B (2011) Analysis of recovery efficiency in a high-temperature energy storage system. Proceedings of the First National Congress on Geothermal Energy, Utrecht, The Netherlands, October 2011
- Hellström G, Tsang CF (1988) Buoyancy flow at a two-fluid interface in a porous medium: analytical studies. *Water Resour Res* 24(4):493–506
- Hellström G, Tsang CF, Claesson J (1979) Heat storage in aquifers: buoyancy flow and thermal stratification problems. Report, Dept. of Math. Phys., Lund Inst. of Technol., Lund, Sweden (also available as Rep. LBL-14246, Lawrence Berkeley Lab., Berkeley, CA)
- Kabus F, Seibt P (2000) Aquifer thermal energy storage for the Berlin Reichstag Building: new seat of the German Parliament. Proceedings of the World Geothermal Congress 2000, Kyushu, Tohoku, Japan, May 28–June 10, 2000
- Kabus F, Hoffman F, Möllmann G (2005) Aquifer storage of waste heat arising from a gas and steam cogeneration plant: concept

- and first operating experience. Proceedings World Geothermal Congress, Antalya, Turkey, April 2005
- Kabus F, Wolfram M, Seibt A, Richlak U, Beuster H (2009) Aquifer thermal energy storage in Neubrandenburg: monitoring throughout three years of regular operation. Proceedings, EFFSTOCK Conference, Stockholm, June 2009, pp 1–8
- Katto Y, Masuoka T (1967) Criterion for the onset of convective flow in a fluid in a porous medium. *Int J Heat Mass Transfer* 10:297–309
- Kipp KL (1987) HST3D: a computer code for simulation of heat and solute transport in three-dimensional ground-water flow systems. *US Geol Surv Water Resour Invest Rep* 86-4095
- Kranz S, Bartels J (2010) Simulation and data based optimisation of an operating seasonal aquifer thermal energy storage. Proceedings World Geothermal Congress, Bali, Indonesia, April 2010
- Lapwood ER (1948) Convection of a fluid in a porous medium. *Proc Camb Phil Soc* 44:508–521
- Nield DA (1975) The onset of transient convective instability. *J Fluid Mech* 71:441–454
- Nield DA, Bejan A (1999) *Convection in porous media*, 2nd edn. Springer, New York
- Sanner B (ed) (1999) High temperature underground thermal energy storage, state-of-the-art and prospects. *Giessener Geol Schrift* 67:1–158
- Sanner B, Kabus F, Seibt P and Bartels J (2005) Underground thermal energy storage for the German Parliament in Berlin, system concept and operational experiences. Proceedings World Geothermal Congress 2005, Antalya, Turkey, April 2005
- Sauty JP, Gringarten AC, Landel PA (1978) The effect of thermal dispersion on injection of hot water in aquifers. Proceedings of the Second Invitational Well Testing Symposium, Berkeley, CA, October 1978
- Sauty JP, Gringarten AC, Menjoz A, Landel PA (1982) Sensible energy storage in aquifers: 1. theoretical study. *Water Resour Res* 18(2):245–252
- Snijders AL (2000) Lessons from 100 ATEs projects: the developments of aquifer storage in the Netherlands. Proceedings of TERRASTOCK 2000, Stuttgart, Germany, August 28–September 1, 2000
- Tan KK, Sam T (1999) Simulations of the onset of transient convection in porous media under fixed surface temperature boundary conditions. Second International Conference on CFD in the Minerals and Process Industries. CSIRO, Melbourne, Australia
- Tsang CF, Buscheck T, Doughty C (1981) Aquifer thermal energy storage: a numerical simulation of Auburn University field experiment. *Water Resour Res* 17(3):647–658
- Ward JD, Simmons CT, Dillon PJ (2007) A theoretical analysis of mixed convection in aquifer storage and recovery: how important are density effects? *J Hydrol* 343:169–186